Edge states in self-complementary checkerboard photonic crystals: Zak phase, surface impedance, and experimental verification

Xiao-Dong Chen, Ding Zhao, Xiao-Sheng Zhu, Fu-Long Shi, Huan Liu, Jin-Cheng Lu, Min Chen, and Jian-Wen Dong*
School of Physics & State Key Laboratory of Optoelectronic Materials and Technologies, Sun Yat-sen University, Guangzhou 510275, China

(Received 17 September 2017; published 19 January 2018)

Edge states of photonic crystals have attracted much attention for the potential applications, such as high transmission waveguide bends, spin-dependent splitters, and one-way photonic circuits. Here, we theoretically discuss and experimentally observe the deterministic edge states in checkerboard photonic crystals. Due to the self-complementarity of checkerboard photonic crystals, a common band gap is structurally protected between two photonic crystals with different unit cells. Deterministic edge states are found inside the common band gap by exploiting the Zak phase analysis and surface impedance calculation. These edge states are also confirmed by a microwave experiment.

DOI: 10.1103/PhysRevA.97.013831

I. INTRODUCTION

Photonic crystals (PCs) are composed of periodic optical structures in which the electromagnetic waves propagate in a similar way as the electrons move inside the periodic potential of semiconductor crystals [1–3]. By carefully designing PCs with various components and structures, the flow of light can be molded in anomalous ways and some fancy photonic phenomena can be observed, e.g., the super-prism [4], the negative refraction [5,6], the sub-λ imaging [7], and the selective transmission [8]. Particularly, edge states in the photonic band gap of PCs have attracted much attention for the confinement and routing of light. For example, the photonic waveguide bend with near 100 percent transmission was achieved by joining three PC straight channels [9]. On-chip unidirectional propagation of spin-polarized light was realized by specially engineering the eigen-fields of edge states in glide-plane photonic crystal slabs [10]. Since edge states are not only theoretically significant but also of application importance, it is desirable to establish the existing conditions of edge states based on firm theories. Recently, between two PCs with different topological invariants, e.g., Zak phase [11–14], Chern number [15–18], spin Chern number [19–22], valley Chern number [23–26], edge states are found due to the topological protection [27–29]. Geometric phase induced edge states were demonstrated in two mutually inverted PCs [30]. Besides, the deterministic edge states between two inverted semi-infinite PCs with slightly disturbed conical dispersions at zone center were theoretically predicted [31] and experimentally observed [32].

To have edge states between two PCs, one condition, i.e., a common band gap, should be satisfied. To obtain a common band gap, the parameters of PCs (e.g., filling ratio and/or permittivity of dielectric medium in the unit cell) should be carefully designed. It will increase the difficulty of theoretical design and experimental fabrication of PC boundary. In this work, we consider the self-complementary checkerboard PC in which the "a common band gap" condition is naturally satisfied without the careful design of the parameters of PCs. Two topologically distinct PCs, i.e., PC1 and PC2, are constructed by different unit cells that are mutually complementary partners. To characterize the presence of edge states, different Zak phases of PC1 and PC2 are obtained and zero surface impedance for the photonic crystal boundary is found. A microwave experiment is also carried out to demonstrate these deterministic edge states.

II. SELF-COMPLEMENTARY CHECKERBOARD PHOTONIC CRYSTAL

Let us start by considering the checkerboard PC shown schematically in Fig. 1(a). It is formed by two interlaced square lattices of dielectric rods with permittivity $\varepsilon_{\text{diel}}$ (black patches) and air rods (white patches). The lattice constant of PC is a, and the side length of dielectric/air rods is $b = a/\sqrt{2}$. As the checkerboard PC is invariant under the interchange of dielectric rods and air rods, it is self-complementary [33]. Due to the self-complementarity, there are two ways to construct the checkerboard PC by choosing different unit cells. The first kind of unit cell is centered at the dielectric rod [outlined by the blue dashed square in Fig. 1(a)]. The PC formed by periodically repeating the dielectric rod centered unit cell is shown in Fig. 1(b), and hereafter we name it as PC1. The other choice is that the unit cell is centered at the air rod (red dashed square). Similarly, PC2 is formed by periodically repeating the air rod centered unit cell [Fig. 1(c)]. Although PC1 and PC2 have different boundary morphologies, they have the same band structures as their infinite structures form the checkerboard PC. As a result, the "a common band gap" condition will be naturally satisfied once a complete or directional band gap is found. Figure 1(d) shows the band structure for the transverse magnetic modes of the checkerboard PC with $\varepsilon_{\text{diel}} = 9$. Between the lowest two bands, there is a complete band gap ranging from $0.245c/a$ to $0.254c/a$ (shaded in green). This band gap is commonly shared by PC1 and PC2, and it serves

*dongjwen@mail.sysu.edu.cn

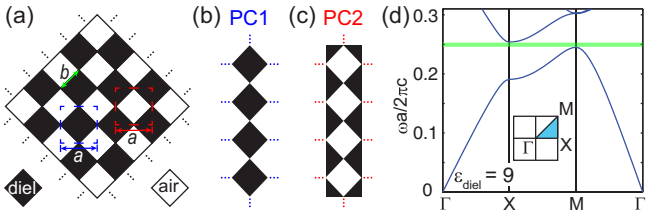

FIG. 1. (a) The schematic of checkerboard PC which consists of two interlaced square lattices of dielectric rods with $\varepsilon_{\text{diel}}$ (black patches) and air rods (white patches). The lattice constant of PC is a, and the side length of rods is $b = a/\sqrt{2}$. Due to the self-complementarity of checkerboard PC, the unit cell can be chosen to be centered at dielectric rod (blue dashed square) or air rod (red dashed square). (b), (c) The schematics of (b) PC1, which is constructed by periodically repeating the dielectric rod centered unit cell, and (c) PC2, which is constructed by periodically repeating the air rod centered unit cell. (d) Band structure for the transverse magnetic modes of the checkerboard PC with $\varepsilon_{\text{diel}} = 9$. The inset shows the first Brillouin zone. A complete band gap ranging from $0.245c/a$ to $0.254c/a$ is highlighted by a green rectangle. This band gap is shared by PC1 and PC2 due to the self-complementarity of checkerboard PC.

as a good starting point to find edge states. Note that although the band width of the complete band gap is small (3.6%), the directional band gap is large enough for the confinement of edge states. For example, the directional band gap along the ΓX direction has a 27.2% gap-midgap ratio.

III. DETERMINISTIC EDGE STATES

A. Zak phase analysis

To study the deterministic edge states at the photonic boundary between PC1 and PC2 (which are inherent in the checkerboard PC), we begin with the discussion about the Zak phase. The reduced 1D band structures for PC1 and PC2 with $k_y = 0.25\pi/a$ are shown in Figs. 2(a) and 2(b), respectively. These band structures are exactly the same due to the self-complementarity of checkerboard PC. But their Zak phases are different. Here the Zak phase of the lowest band can be obtained by considering the symmetries of eigen-states at two high symmetry k-points in the reduced 1D Brillouin zone, i.e., $k_x = -\pi/a$ (labeled by A) and $k_x = 0$ (labeled by B) [30,34]. Kohn's results [34] tell us that if either $|\tilde{E}_{\text{A}}(x=0)|$ or $|\tilde{E}_{\text{B}}(x=0)|$ is equal to zero while the other one is nonzero, the Zak phase is π; otherwise the Zak phase is 0. Here, $\tilde{E}_{\vec{k}}(x=0)$ is defined as $\tilde{E}_{\vec{k}}(x=0) = \frac{1}{a}\int_0^a E_{\vec{k}}(0,y)e^{-ik_y\cdot y}dy$, where the subscript $\vec{k}$ is considered at A or B points, and the electric fields at $x = 0$ are integrated. For example, the electric fields of eigen-states at A and B points for PC1 are shown in the middle insets of Fig. 2(a). After the numerical summation, we found that $|\tilde{E}_{\text{A}}(x=0)| = 0$ while $|\tilde{E}_{\text{B}}(x=0)| \neq 0$ (Note that $|\tilde{E}_{\text{A}}(x=0)| = 0$ can be obtained by inspecting two conditions, i.e., the symmetric condition and the periodic condition, imposing on the electric fields at $x = 0$ and $x = a$). Therefore, the Zak phase is π, which is given along with the band structure shown in Fig. 2(a). On the other hand, the Zak phase of the lowest bulk band of PC2 is 0 as both $|\tilde{E}_{\text{A}}(x=0)|$ and $|\tilde{E}_{\text{B}}(x=0)|$ are nonzero [Fig. 2(b)]. Hence, we conclude that the first bands of PC1 and PC2 have different Zak phases. When the band gap above the first bulk band is considered, deterministic edge states can be found at the boundary between these two PCs with different Zak phases [30]. To see this, we consider the photonic boundary shown in the inset of Fig. 2(c). On the left-hand side of this boundary is the semi-infinite PC1 while on the right-hand side is the semi-infinite PC2. This photonic boundary is periodic along the y direction and its

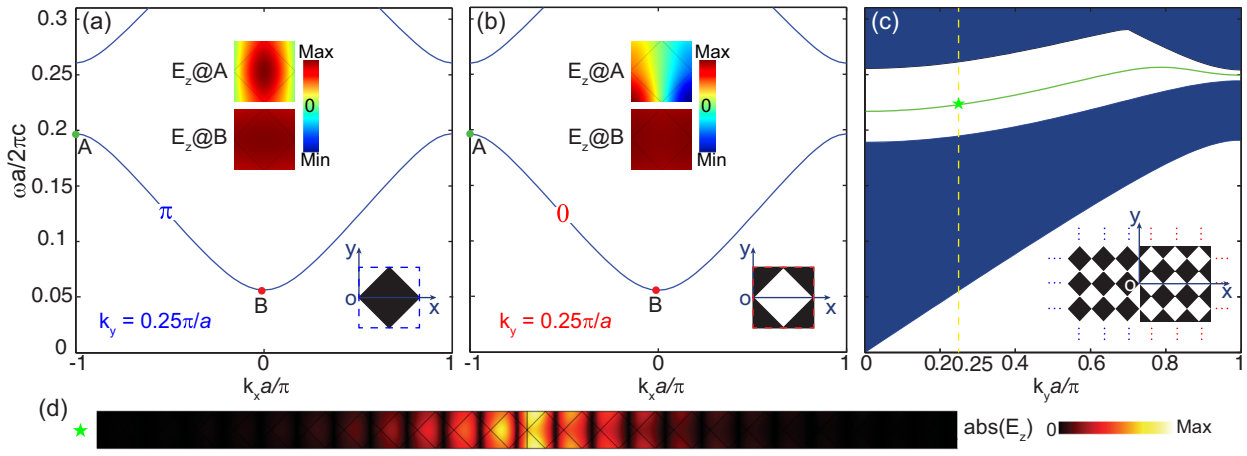

FIG. 2. Zak phase analysis. (a) Band structure, eigen-fields and Zak phase for PC1 whose unit cell is centered at dielectric rod. The schematic of the unit cell is shown in the right inset. The coordinate origin is located at the center of the left boundary of the unit cell. The middle inset shows the electric fields of two eigen-states at high symmetry A point ($k_x = -\pi/a$) and B point ($k_x = 0$). As $|\tilde{E}_{\text{A}}(x=0)| = 0$ and $|\tilde{E}_{\text{B}}(x=0)| \neq 0$, the Zak phase is π which is given along with the reduced 1D band structure for $k_y = 0.25\pi/a$. (b) Band structure, eigen-fields, and Zak phase for PC2 whose unit cell is centered at air rod. Due to different field distributions of eigen-states at A point comparing to those of PC1, the Zak phase for PC2 changes to be 0. (c) Projected band structures for the photonic boundary between the semi-infinite PC1 and PC2. The green line represents edge states dispersion, and the inset shows the schematic of photonic boundary. (d) The amplitude of electric fields of one representative edge state with $f = 0.223c/a$ at $k_y = 0.25\pi/a$ [marked by a green star in (c)]. Fields are localized near the boundary.

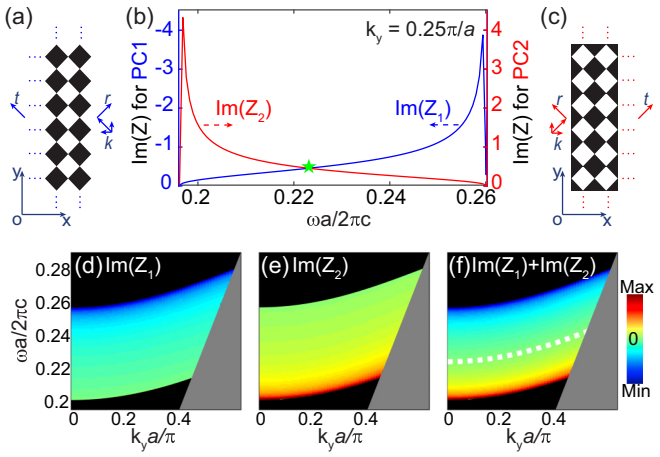

FIG. 3. Surface impedance calculation. The schemetics of (a) the semi-infinite PC1 and (c) the semi-infinite PC2 for the transmission simulation. (b) The value of Im(Z) for PC1 (i.e., Im(Z_1) and marked in blue) and Im(Z) for PC2 (i.e., Im(Z_2) and marked in red) as a function of frequency. The tangential component of incident wavevector is $k_y = 0.25\pi/a$. One edge state exists at $f = 0.223c/a$ at which the zero-impedance condition $\mathrm{Im}(Z_1) + \mathrm{Im}(Z_2) = 0$ is fulfilled (green star). (d) Distribution of surface impedance $\mathrm{Im}(Z_1(\omega,k_y))$ for PC1. (e) Distribution of surface impedance $\mathrm{Im}(Z_2(\omega,k_y))$ for PC2. (f) Distribution of $\mathrm{Im}(Z_1) + \mathrm{Im}(Z_2)$. For each k_y, $\mathrm{Im}(Z_1) + \mathrm{Im}(Z_2)$ drops monotonically from $+\infty$ to $-\infty$ with the increasing frequency, and goes across the value of zero. A white-dashed line outlines the positions (ω,k_y), where $\mathrm{Im}(Z_1) + \mathrm{Im}(Z_2) = 0$ is fulfilled.

corresponding band structure is given in Fig. 2(c). Ingrained from the self-complementarity of checkerboard PC, a common band gap is found (shaded in white). Accompanied with the appearance of this common band gap, edge states expanding from $k_y = 0$ to $k_y = \pi/a$ also appear (marked in green). Figure 2(d) plots the amplitude of electric fields of one representative edge state with $f = 0.223c/a$ at $k_y = 0.25\pi/a$ [marked by a green star in Fig. 2(c)]. The edge state localizes around the boundary and decays exponentially away from the boundary. For other values of k_y, edge states are also found in this photonic boundary with two constituent PCs having different Zak phases.

B. Surface impedance calculation

Besides analyzing the Zak phase, the surface impedance calculation is another method to determine whether the edge states appear or not at the photonic boundary [35]. With the theoretical and experimental results, a universal zero-impedance condition has been found for two kinds of localized interface modes in the whole momentum space (both above and below the light line) [35]. Here, we obtain the surface impedance by the well-established retrieval method from scattering parameters [36,37]. As schematically shown in Figs. 3(a) and 3(c), plane waves are incident with the wave vector ($\boldsymbol{k}$), and periodic boundary conditions are applied along the y direction. In principle, a semi-infinite stack of layers should be employed along the x direction. But in the simulation, the value of surface impedance inside the band gap converges to a constant when the number of layer is as many as 30. The reflection (r) and transmission (t) coefficients are exacted and the surface impedance Z can be obtained [36–38]:

$$\mathrm{Z}(\omega,k_y) = \pm\frac{\sqrt{(1+r)^2 - t^2}}{\sqrt{(1-r)^2 - t^2}\sqrt{1 - k_y^2/k^2}}, \qquad (1)$$

where k is the amplitude of $\boldsymbol{k}$, and k_y is the tangential component of $\boldsymbol{k}$ along the boundary. The sign of surface impedance in Eq. (1) can be determined by the causality consideration: the real part of surface impedance [i.e., Re(Z)] should be larger than or equal to zero. Inside the band gap, Re(Z) goes to zero and the imaginary part of surface impedance [i.e., Im(Z)] determines how the waves reflect and transmit across the boundary. For example, Fig. 3(b) plots the variation of Im(Z) for a given $k_y = 0.25\pi/a$ as a function of frequency. For PC1, the value of Im(Z_1) decreases monotonically from 0 to about -4 with the increasing frequency inside the directional band gap ranging from $0.194c/a$ to $0.262c/a$ [see the blue curve in Fig. 3(b)]. Whereas for PC2, the value of Im(Z_2) decreases monotonically from about 4 to 0 with the increasing frequency [see the red curve in Fig. 3(b)]. Due to the opposite signs between Im(Z_1) and Im(Z_2) and their monotonicity, the zero surface impedance condition of $\mathrm{Im}(Z_1) + \mathrm{Im}(Z_2) = 0$ can be achieved at a particular frequency. At this frequency, one edge state of photonic boundary can be found. As marked by the green star at which $\mathrm{Im}(Z_1) + \mathrm{Im}(Z_2) = 0$ is fulfilled, the edge state exists at $f = 0.223c/a$ [Fig. 3(b)]. It is in good agreement with the frequency obtained by the full-wave calculations shown in Fig. 2(d).

For generality, Figs. 3(d) and 3(e), respectively, show Im(Z_1) and Im(Z_2) in the ω-k_y diagram. Here the surface impedance for electromagnetic waves inside the directional band gap is given as we try to find edge states in the band gap. Also, only the surface impedance for the extended states locating above the light line is given as the evanescent waves below the light line (shaded in gray) are not considered. For PC1, Im(Z_1) decreases monotonically from 0 to $-\infty$ with the increasing frequency [Fig. 3(d)], while Im(Z_2) decreases monotonically from $+\infty$ to 0 for PC2 [Fig. 3(e)]. To find out the frequencies at which the zero surface impedance condition will be fulfilled, we plot $\mathrm{Im}(Z_1) + \mathrm{Im}(Z_2)$ in Fig. 3(f). For each k_y, $\mathrm{Im}(Z_1) + \mathrm{Im}(Z_2)$ drops monotonically from $+\infty$ to $-\infty$ with the increasing frequency. It will definitely go across the value of 0, and it implies that there exists one edge state inside the common band gap. This is confirmed by the white dashed curve in Fig. 3(f) where $\mathrm{Im}(Z_1) + \mathrm{Im}(Z_2) = 0$ is plot. It is in good agreement with the edge dispersion obtained by the full-wave calculations shown in Fig. 2(c).

Note that the Zak phase of the first bulk band (i.e., φ) and the surface impedance of the first and second lowest band gap (i.e., Z_{gap1} and Z_{gap2}) are closely related [11,31]:

$$\mathrm{sgn}[\mathrm{Im}(Z_{\mathrm{gap2}})]/\mathrm{sgn}[\mathrm{Im}(Z_{\mathrm{gap1}})] = -\exp(i\varphi). \qquad (2)$$

As the sign of the first lowest band gap is always negative [31], the sign of the second lowest band gap can be obtained by $\mathrm{sgn}[\mathrm{Im}(Z_{\mathrm{gap2}})] = \exp(i\varphi)$. This relation is verified by the results shown in Figs. 2 and 3. For example, the Zak phase of the first bulk band of PC1 is π (i.e., $\varphi = \pi$), hence $\mathrm{sgn}[\mathrm{Im}(Z_{\mathrm{gap2}})] = -1$. This is confirmed by the negative values of Im(Z_1) shown in Fig. 3(d). On the contrary, $\varphi = 0$ and

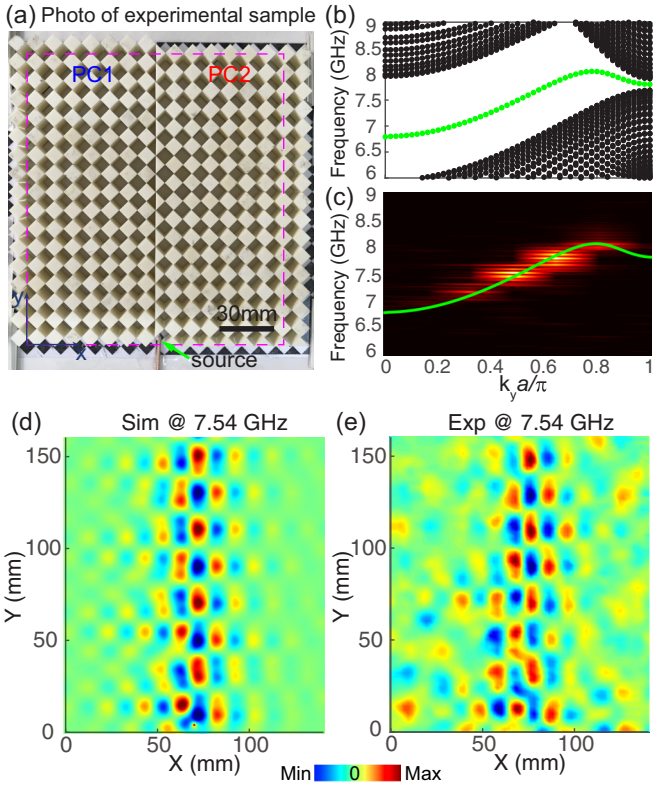

FIG. 4. Microwave experimental verification. (a) Photo of experimental sample with PC1 on the left and PC2 on the right. The dielectric rod is alumina rod with $\varepsilon_{\text{diel}} = 8.2$, and the lattice constant of PC is $a = 10\,\text{mm}$. A pink dashed rectangle outlines the scanned region in the experiment, and a green arrow marks the monopole source. (b) Calculated projected bands (black) and edge states (green) dispersions for the boundary shown in (a). (c) Measured dispersions (bright color) for the deterministic edge states, compared with the numerical data (green line). (d) The simulated and (e) measured E_z fields of edge states at the frequency of 7.54 GHz.

$\text{sgn}[\text{Im}(Z_{\text{gap2}})] = 1$ for PC2. So we find the positive values of $\text{Im}(Z_2)$ in Fig. 3(e).

C. Microwave experimental verification

To prove the existence of edge states predicted by both the Zak phase analysis and surface impedance calculation, a microwave experiment is carried out. Figure 4(a) shows the photo of the experimental sample with PC1 locating on the left and PC2 on the right. Due to the similarity between the TM_0 modes of 3D waveguide and TM modes of 2D system, these PC arrays are sandwiched between two parallel perfect electric conductor plates (not shown). The lattice constant is $a = 10\,\text{mm}$ for both two PCs. The relative permittivity of dielectric squared rod (alumina) is $\varepsilon_{\text{diel}} = 8.2$, which is smaller than expected due to the fabrication defect. But note that the reduction of permittivity of dielectric rods does not change the Zak phase and the sign of $\text{Im}(Z)$ of each PC, and hence the deterministic edge states still exist. To see this, the projected band structures of two PCs and the edge state dispersions along the k_y direction are shown in Fig. 4(b). Due to the self-complementarity of checkerboard PC, PC1 and PC2 share the same projected bulk bands (shaded in black). Inside the common directional band gap (white region), deterministic edge states are found [marked in green in Fig. 4(b)]. As to excite these edge states, a monopole source is placed at the bottom of the boundary [outlined by a green arrow in Fig. 4(a)]. It emits electromagnetic waves with various wave-vectors and excites the upwards propagating edge states along the photonic boundary. This monopole source and PC sample are put on the bottom perfect electric conductor plate which is stationary during the measurement. On the contrary, the top plate is mounted on a two dimensional (xy plane) motorized translation stage. A hole is drilled in the top plate, and a scanning antenna is inserted to record the electric fields. All the signals are collected by the vector network analyzer [39], which is connected to both source and detective antennas. As an example, the experimentally measured E_z field of edge state at 7.54 GHz is shown in Fig. 4(e). Here, the measured region is limited to $140 \times 160\,\text{mm}^2$ due to the finite size of the experimental sample. The electric field is confined at the boundary ($x = 70\,\text{mm}$) and decay away from the boundary. It is in good agreement with the numerical simulation result shown in Fig. 4(d). In addition, we perform the fast Fourier transform on the measured fields to retrieve the wave vectors of excited edge states. As shown in Fig. 4(c), the dark and bright colors indicate low and high Fourier amplitudes, respectively. The experimental data (bright color) capture well the numerical dispersions (green line) for the deterministic edge states. Note that edge states around 6.8 GHz are not excited due to the small group velocity for edge states near k_y from 0 to $0.2\pi/a$.

IV. CONCLUSION

In conclusion, by employing the self-complementary feature of the checkerboard PC, "a common band gap" condition for finding edge states is naturally satisfied between two PCs, which are constructed by different unit cells. Inside the common band gap, the deterministic edge states are found under both the Zak phase analysis and the surface impedance calculation. Last, a microwave experiment is also carried out to demonstrate these deterministic edge states.

ACKNOWLEDGEMENTS

This work is supported by Natural Science Foundation of China (Grants No. 11522437, No. 11704422, and No. 61775243), Guangdong Natural Science Funds for Distinguished Young Scholar (Grant No. S2013050015694), Guangdong Special Support Program, and Fundamental Research Funds for the Central Universities (Grant No.17lgpy19).

[1] E. Yablonovitch, Inhibited Spontaneous Emission in Solid-State Physics and Electronics, Phys. Rev. Lett. **58**, 2059 (1987).

[2] S. John, Strong Localization of Photons in Certain Disordered Dielectric Superlattices, Phys. Rev. Lett. **58**, 2486 (1987).

[3] J. D. Joannopoulos, S. G. Johnson, J. N. Winn, and R. D. Meade, *Photonic Crystals—Molding the Flow of Light* (Princeton University Press, Princeton, NJ, 2008).

[4] H. Kosaka, T. Kawashima, A. Tomita, M. Notomi, T. Tamamura, T. Sato, and S. Kawakami, Photonic crystals for micro lightwave circuits using wavelength-dependent angular beam steering, Appl. Phys. Lett. **74**, 1370 (1999).

[5] M. Notomi, Theory of light propagation in strongly modulated photonic crystals: Refractionlike behavior in the vicinity of the photonic band gap, Phys. Rev. B **62**, 10696 (2000).

[6] Y. Poo, C. He, C. Xiao, M. H. Lu, R. X. Wu, and Y. F. Chen, Manipulating one-way space wave and its refraction by time-reversal and parity symmetry breaking, Sci. Rep. **6**, 29380 (2016).

[7] C. Luo, S. G. Johnson, J. D. Joannopoulos, and J. B. Pendry, All-angle negative refraction without negative effective index, Phys. Rev. B **65**, 201104 (2002).

[8] Y. Shen, D. Ye, I. Celanovic, S. G. Johnson, J. D. Joannopoulos, and M. Soljačić, Optical broadband angular selectivity, Science **343**, 1499 (2014).

[9] S.-Y. Lin, E. Chow, V. Hietala, P. R. Villeneuve, and J. D. Joannopoulos, Experimental demonstration of guiding and bending of electromagnetic waves in a photonic crystal, Science **282**, 274 (1988).

[10] I. Söllner, S. Mahmoodian, S. L. Hansen, L. Midolo, A. Javadi, G. Kiršanskė, T. Pregnolato, H. El-Ella, E. H. Lee, J. D. Song, S. Stobbe, and P. Lodahl, Deterministic photon-emitter coupling in chiral photonic circuits, Nat. Nanotechnol. **10**, 775 (2015).

[11] M. Xiao, Z. Q. Zhang, and C. T. Chan, Surface Impedance and Bulk Band Geometric Phases in One-Dimensional Systems, Phys. Rev. X **4**, 021017 (2014).

[12] Q. Wang, M. Xiao, H. Liu, S. Zhu, and C. T. Chan, Measurement of the Zak phase of photonic bands through the interface states of a metasurface/photonic crystal, Phys. Rev. B **93**, 041415 (2016).

[13] X. Shi, C. Xue, H. Jiang, and H. Chen, Topological description for gaps of one-dimensional symmetric all-dielectric photonic crystals, Opt. Express **24**, 18580 (2016).

[14] Y. Yang, T. Xu, Y. F. Xu, and Z. H. Hang, Zak phase induced multiband waveguide by two-dimensional photonic crystals, Opt. Lett. **42**, 3085 (2017).

[15] F. D. M. Haldane, and S. Raghu, Possible Realization of Directional Optical Waveguides in Photonic Crystals with Broken Time-Reversal Symmetry, Phys. Rev. Lett. **100**, 013904 (2008).

[16] Z. Wang, Y. D. Chong, J. D. Joannopoulos, and M. Soljačić, Reflection-Free One-Way Edge Modes in a Gyromagnetic Photonic Crystal, Phys. Rev. Lett. **100**, 013905 (2008).

[17] Y. Poo, R.-x. Wu, Z. Lin, Y. Yang, and C. T. Chan, Experimental Realization of Self-Guiding Unidirectional Electromagnetic Edge States, Phys. Rev. Lett. **106**, 093903 (2011).

[18] S. A. Skirlo, L. Lu, Y. Igarashi, Q. Yan, J. Joannopoulos, and M. Soljačić, Experimental Observation of Large Chern Numbers in Photonic Crystals, Phys. Rev. Lett. **115**, 253901 (2015).

[19] A. B. Khanikaev, S. H. Mousavi, W.-K. Tse, M. Kargarian, A. H. MacDonald, and G. Shvets, Photonic topological insulators, Nat. Mater. **12**, 233 (2012).

[20] W.-J. Chen, S.-J. Jiang, X.-D. Chen, B. Zhu, L. Zhou, J.-W. Dong, and C. T. Chan, Experimental realization of photonic topological insulator in a uniaxial metacrystal waveguide, Nat. Commun. **5**, 5782 (2014).

[21] T. Ma, A. B. Khanikaev, S. H. Mousavi, and G. Shvets, Guiding Electromagnetic Waves Around Sharp Corners: Topologically Protected Photonic Transport in Metawaveguides, Phys. Rev. Lett. **114**, 127401 (2015).

[22] L.-H. Wu, and X. Hu, Scheme for Achieving a Topological Photonic Crystal by Using Dielectric Material, Phys. Rev. Lett. **114**, 223901 (2015).

[23] T. Ma, and G. Shvets, All-si valley-Hall photonic topological insulator, New J. Phys. **18**, 025012 (2016).

[24] X.-D. Chen, F.-L. Zhao, M. Chen, and J.-W. Dong, Valley-contrasting physics in all-dielectric photonic crystals: Orbital angular momentum and topological propagation, Phys. Rev. B **96**, 020202(R) (2017).

[25] M. J. Collins, F. Zhang, R. Bojko, L. Chrostowski, and M. C. Rechtsman, Integrated optical Dirac physics via inversion symmetry breaking, Phys. Rev. A **94**, 063827 (2016).

[26] R. K. Pal, and M. Ruzzene, Edge waves in plates with resonators: An elastic analogue of the quantum valley Hall effect, New J. Phys. **19**, 025001 (2017).

[27] L. Lu, J. D. Joannopoulos, and M. Soljačić, Topological photonics, Nat. Photon. **8**, 821 (2014).

[28] X.-C. Sun, C. He, X.-P. Liu, M.-H. Lu, S.-N. Zhu, and Y.-F. Chen, Two-dimensional topological photonic systems, Prog. Quantum Electron. **55**, 52 (2017).

[29] Y. Wu, C. Li, X. Hu, Y. Ao, Y. Zhao, and Q. Gong, Applications of Topological Photonics in Integrated Photonic Devices, Adv. Opt. Mater. **5**, 1700357 (2017).

[30] X. Huang, Y. Yang, Z. H. Hang, Z.-Q. Zhang, and C. T. Chan, Geometric phase induced interface states in mutually inverted two-dimensional photonic crystals, Phys. Rev. B **93**, 085415 (2016).

[31] X. Huang, M. Xiao, Z.-Q. Zhang, and C. T. Chan, Sufficient condition for the existence of interface states in some two-dimensional photonic crystals, Phys. Rev. B **90**, 075423 (2014).

[32] Y. Yang, X. Huang, and Z. H. Hang, Experimental Characterization of the Deterministic Interface States in Two-Dimensional Photonic Crystals, Phys. Rev. Appl. **5**, 034009 (2016).

[33] M. Senechal, Color symmetry, Comput. Math. Appl. **16**, 545 (1988).

[34] W. Kohn, Analytic properties of Bloch waves and Wannier Functions, Phys. Rev. **115**, 809 (1959).

[35] J. W. Dong, J. Zeng, Q. F. Dai, and H. Z. Wang, Universal condition for the existence of interface modes in the whole momentum space with arbitrary materials, arXiv:0801.4117.

[36] X. Chen, T. M. Grzegorczyk, B.-I. Wu, J. Pacheco, and J. A. Kong, Robust method to retrieve the constitutive effective parameters of metamaterials, Phys. Rev. E **70**, 016608 (2004).

[37] D. R. Smith, D. C. Vier, T. Koschny, and C. M. Soukoulis, Electromagnetic parameter retrieval from inhomogeneous metamaterials, Phys. Rev. E **71**, 036617 (2005).

[38] Y. Zhou, X.-T. He, F.-L. Zhao, and J.-W. Dong, Proposal for achieving in-plane magnetic mirrors by silicon photonic crystals, Opt. Lett. **41**, 2209 (2016).

[39] Agilent E5071C.